Electronic Supplementary Material (ESI) for Nanoscale.

Supporting Information

High-performance Si@C anode for lithium-ion batteries enabled by a novel structuring strategy

Jian Song[a], Shengfeng Ke[a], Pengkai Sun[a], Dian Yang[a], Chengang Luo[a], Qinghua Tian[a], Liang Cui[a] and Jizhang Chen[b]*

[a]Key Laboratory of Surface & Interface Science of Polymer Materials of Zhejiang Province, School of Chemistry and Chemical Engineering, Zhejiang Sci-Tech University, Hangzhou, 310018, P. R. China

[b]College of Materials Science and Engineering, Nanjing Forestry University, Nanjing, 210037, P. R. China

**Corresponding author e-mail addresses: 09tqinghua@163.com*

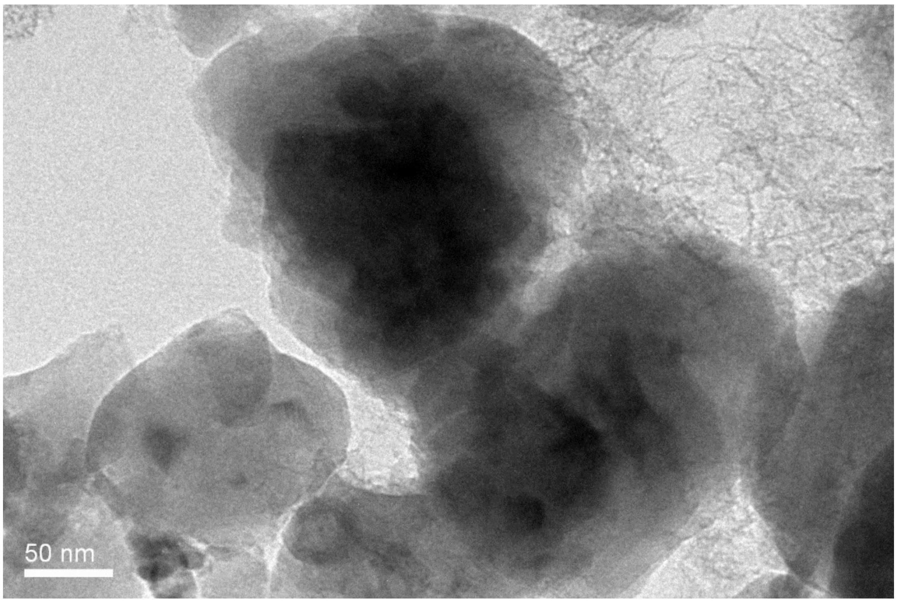

Fig. S1 *TEM image of Si@FeNO.*

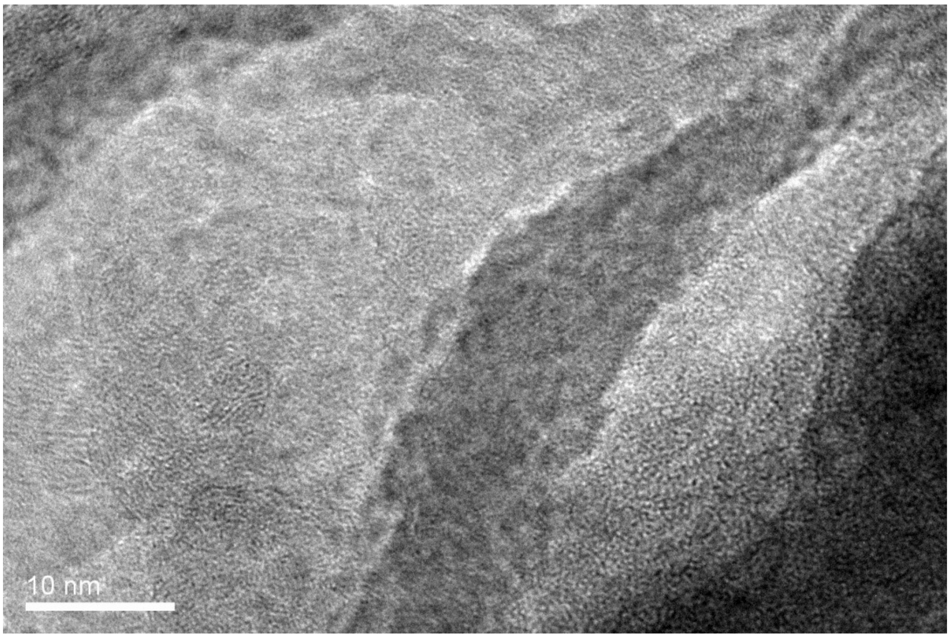

Fig. S2 *TEM image of PVP-derived carbon in Si@P.*

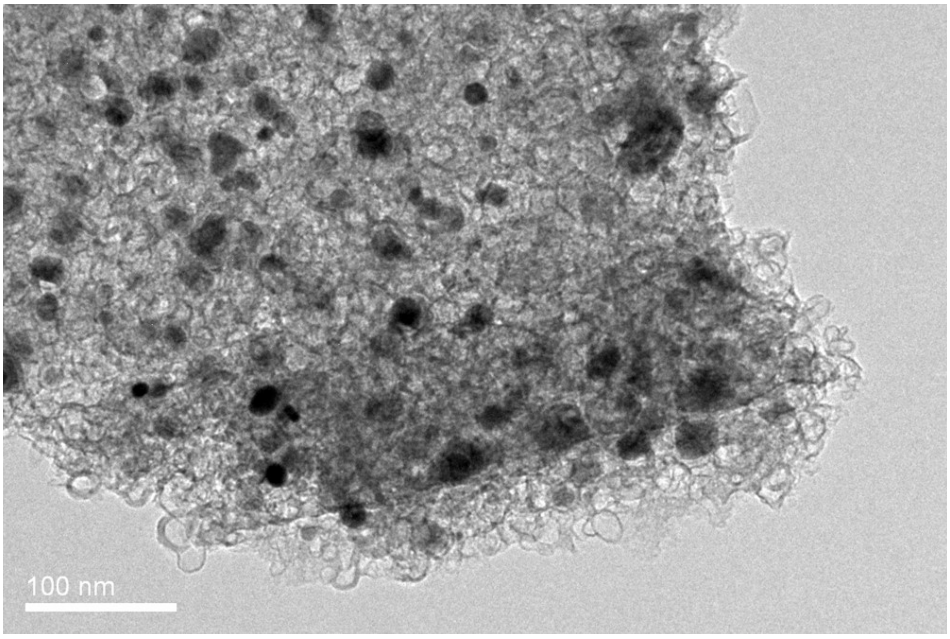

Fig. S3 *TEM image of FeNO@P.*

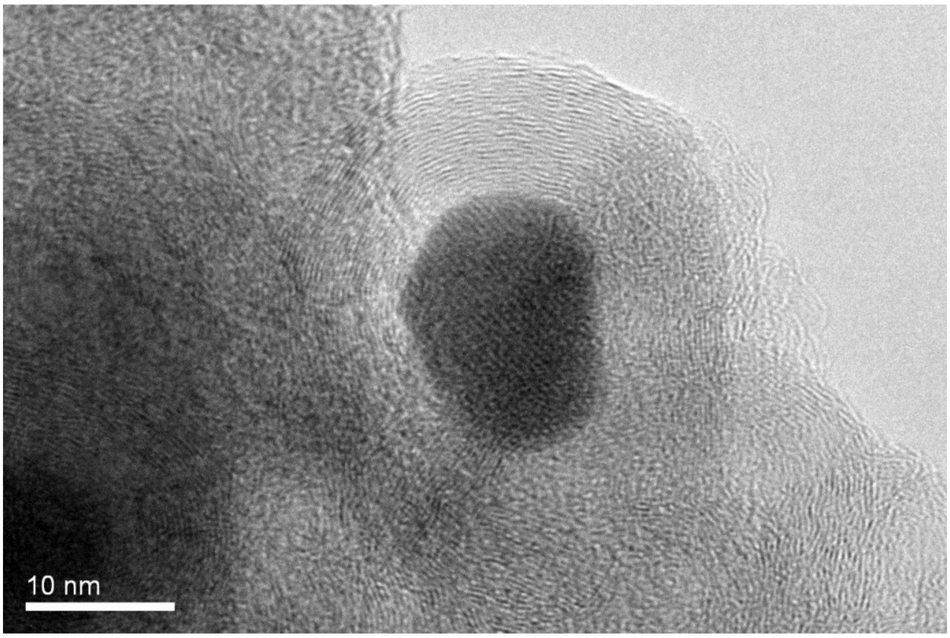

Fig. S4 *HRTEM image of FeNO@P.*

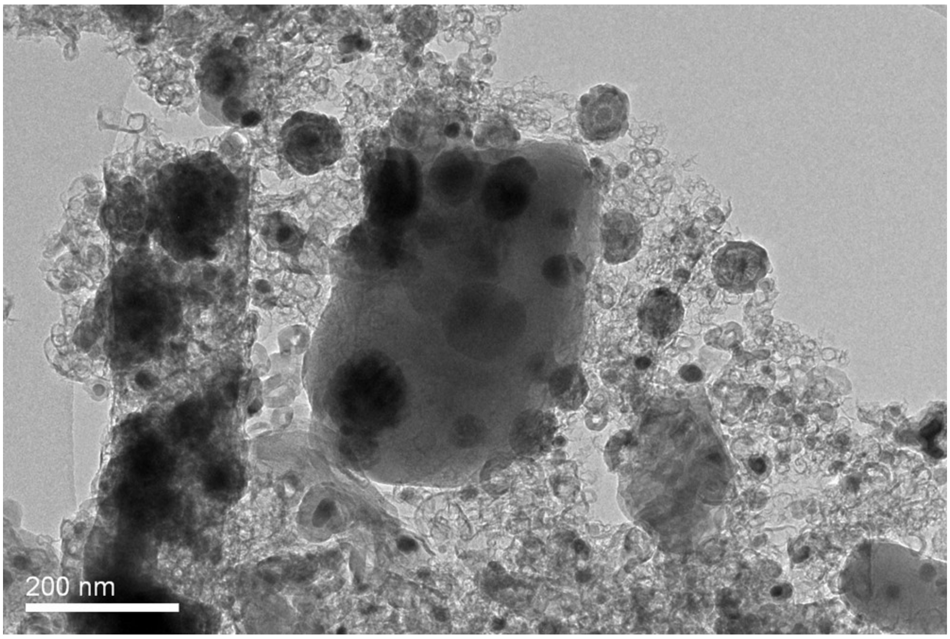

Fig. S5 *TEM image of Si@FeNO@P.*

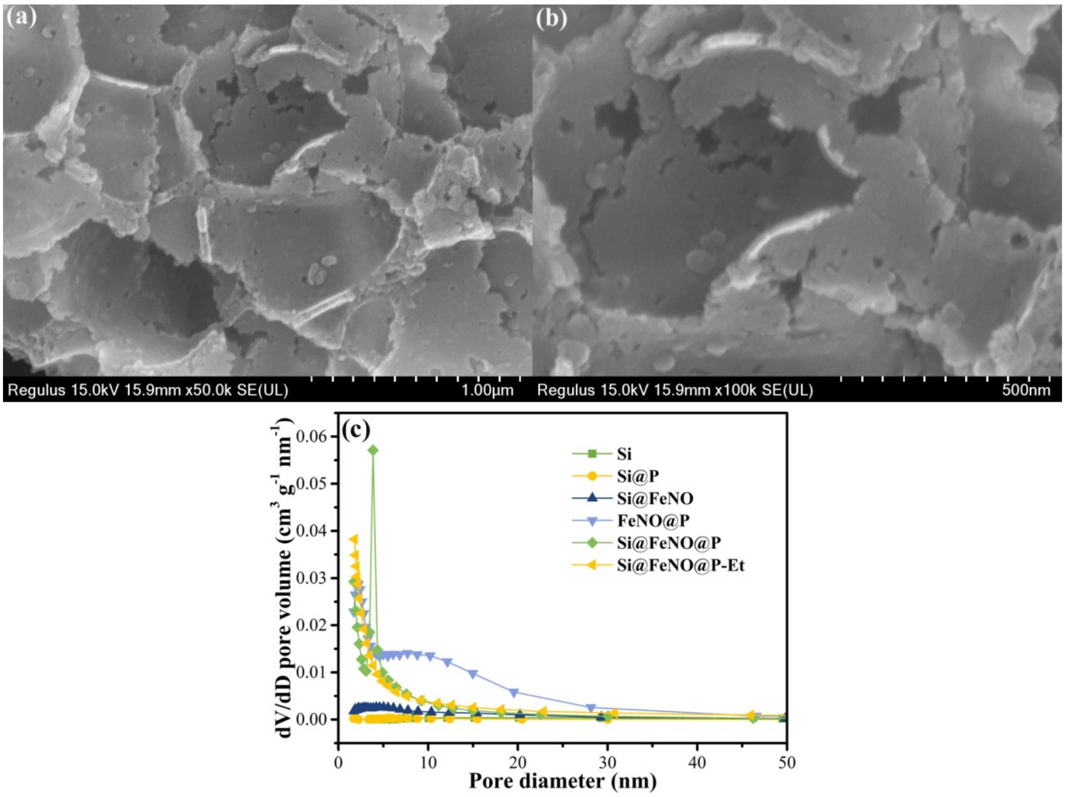

Fig. S6 *SEM images of Si@FeNO@P with (a) 50K and (b) 100K magnifications. (c) Pore size distribution curves of different samples.*

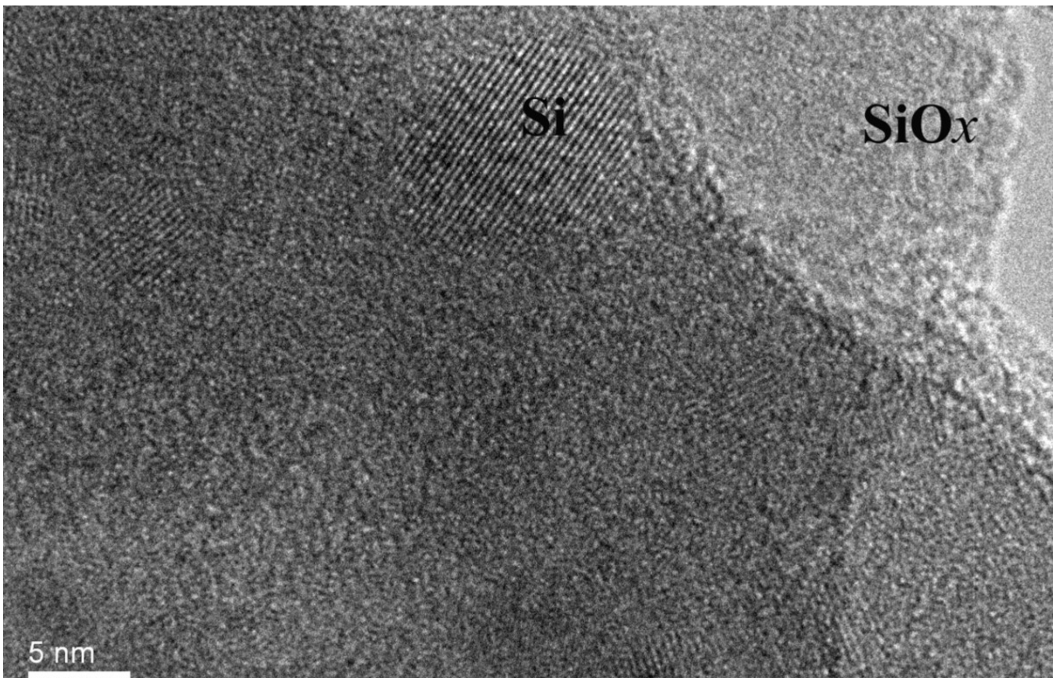

Fig. S7 *HRTEM image of the pure Si nanoparticles.*

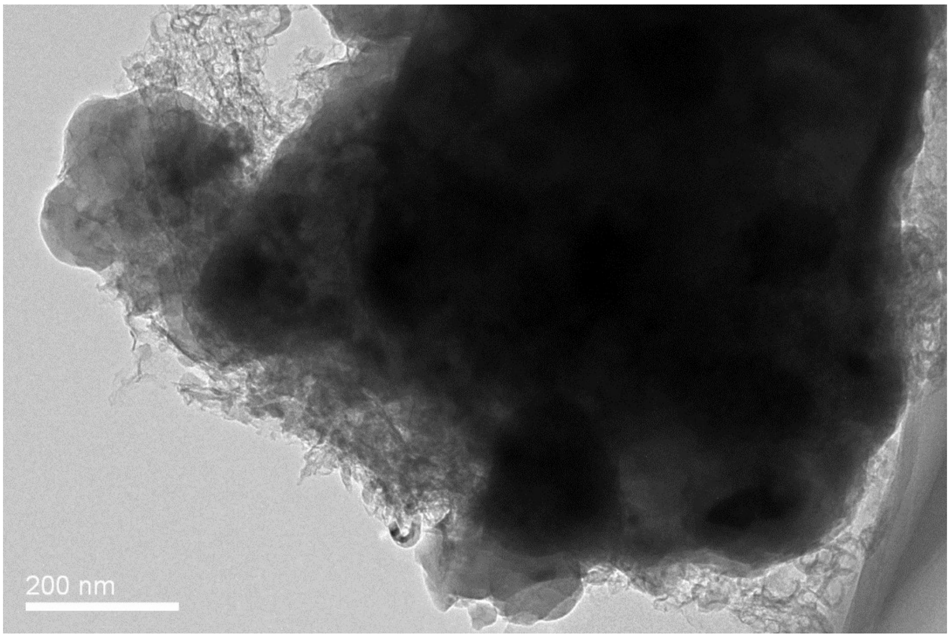

Fig. S8 *TEM image of Si@FeNO@P-Et.*

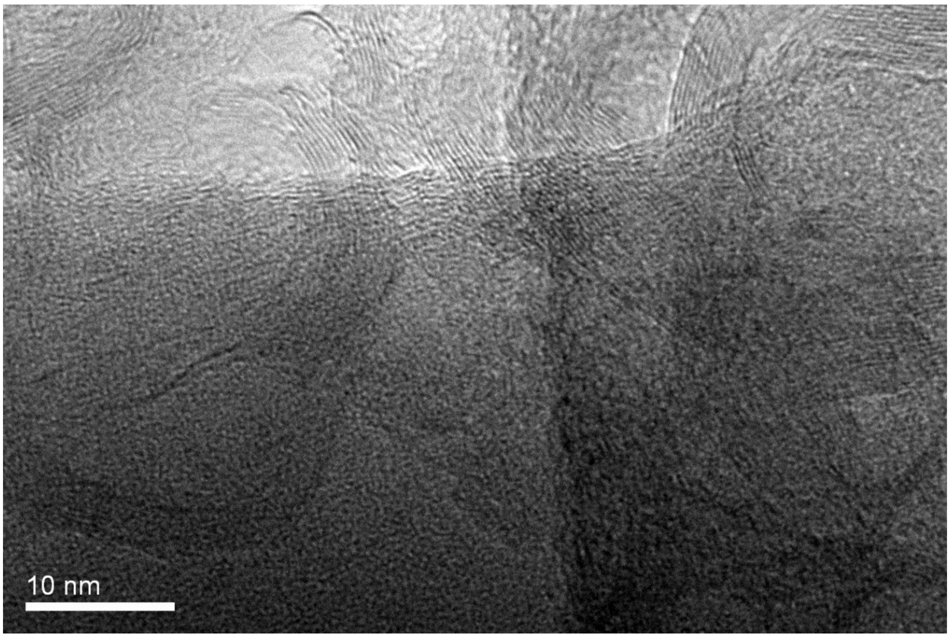

Fig. S9 *HRTEM image of carbon of Si@FeNO@P-Et.*

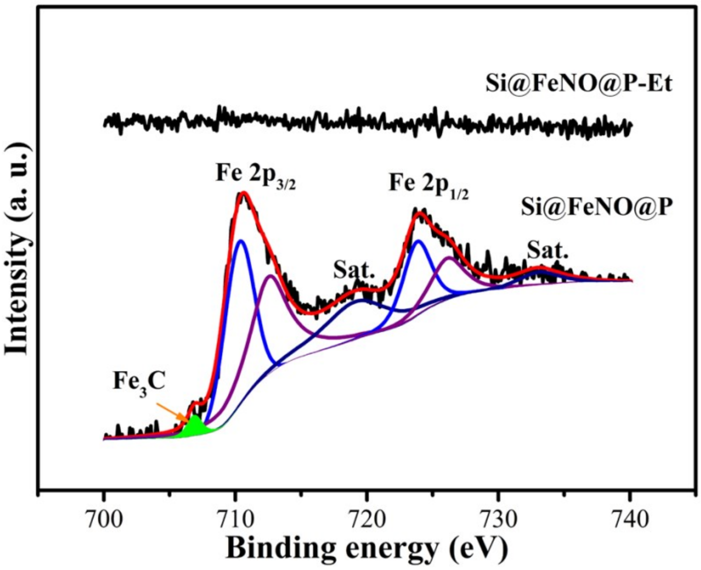

Fig. S10 *Fe 2p HRXPS spectra of Si@FeNO@P and Si@FeNO@P-Et.*

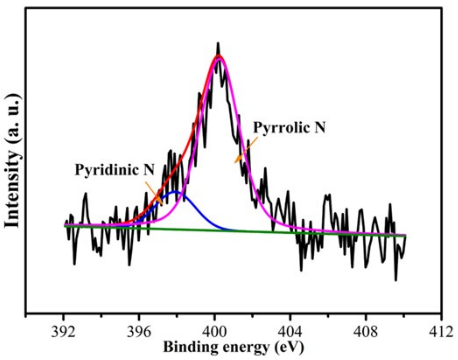

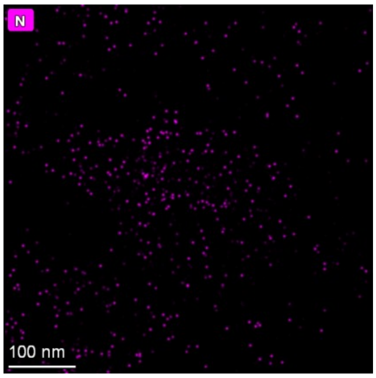

Fig. S11 *N 1s HRXPS spectra and N elemental mapping (based on Fig. 2j) of Si@FeNO@P.*

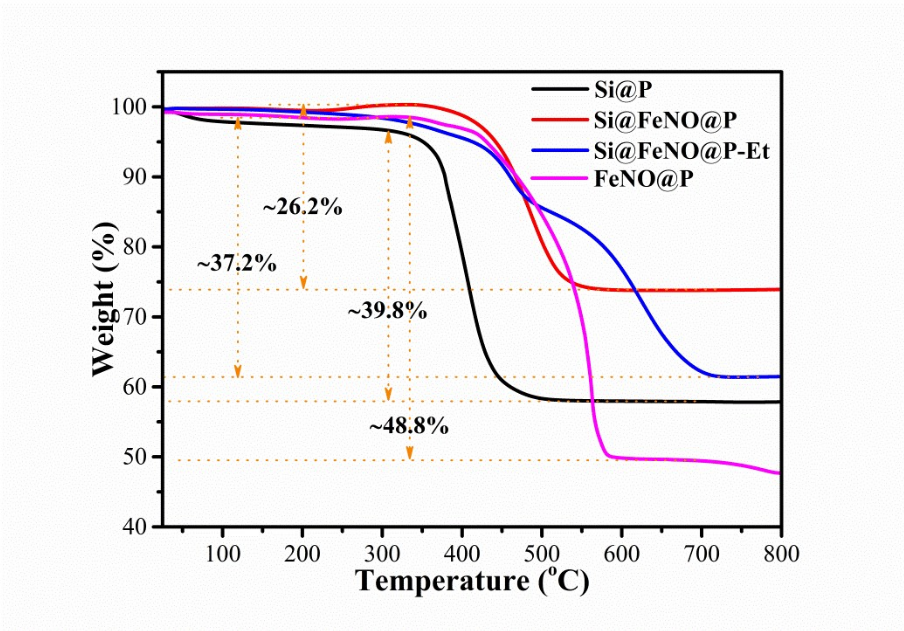

Fig. S12 *TG curves of different samples at 10 ℃/min from room temperature to 800 ℃.*

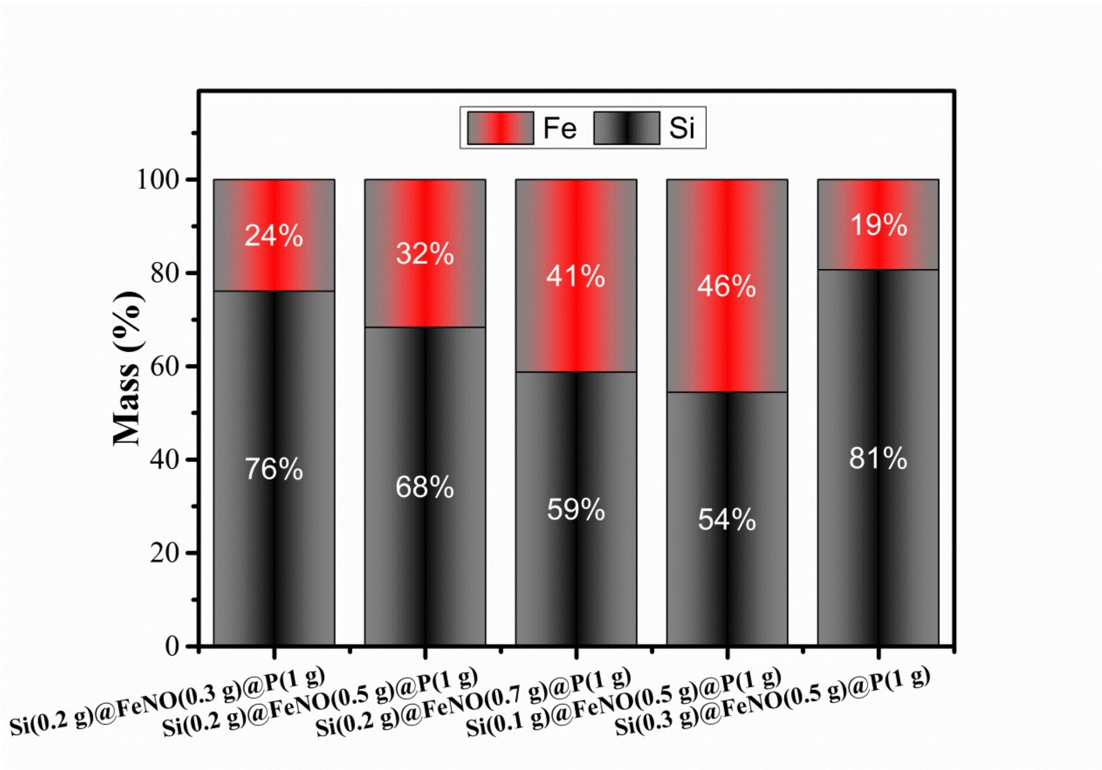

Fig. S13 *Mass ratios of Fe to Si of different samples obtained ICP characterization.*

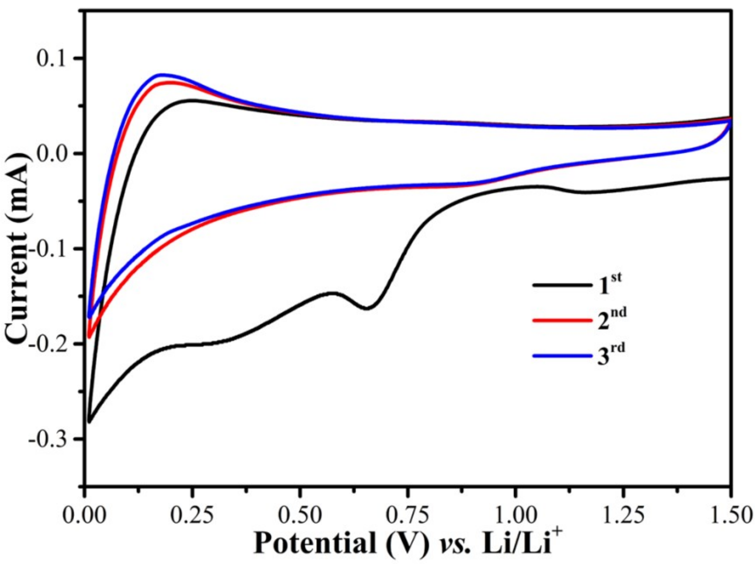

Fig. S14 *CVs of FeNO@P at 0.3 mV s⁻¹ between 0.01 and 1.5 V.*

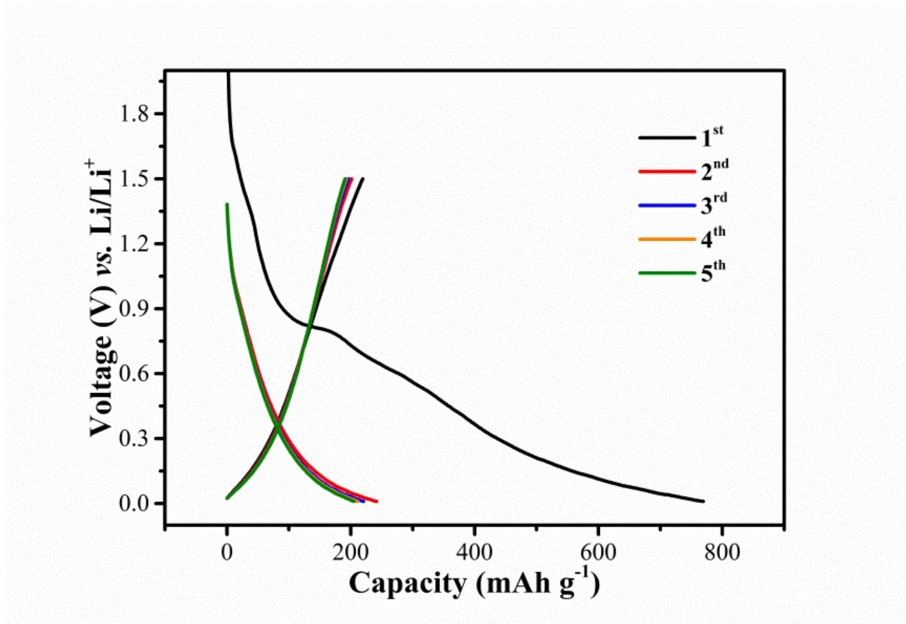

Fig. S15 *Galvanostatic charge/discharge profiles of FeNO@P at 100 mA* g^{-1}.

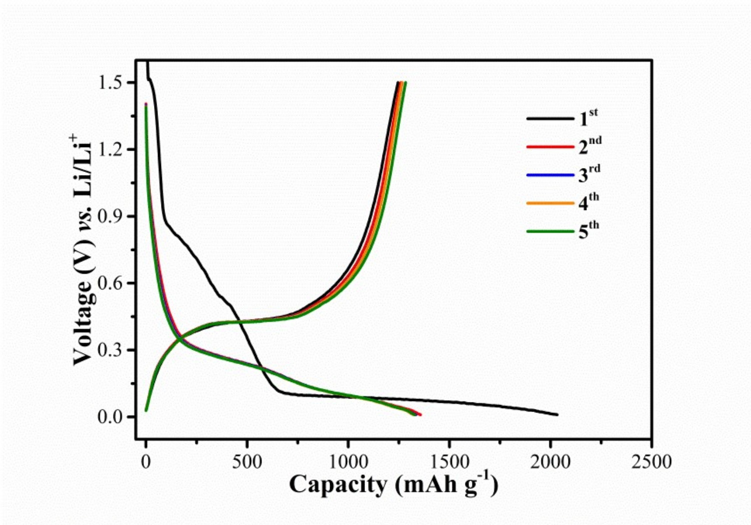

Fig. S16 *Galvanostatic charge/discharge profiles of Si@FeNO at 100 mA g*$^{-1}$.

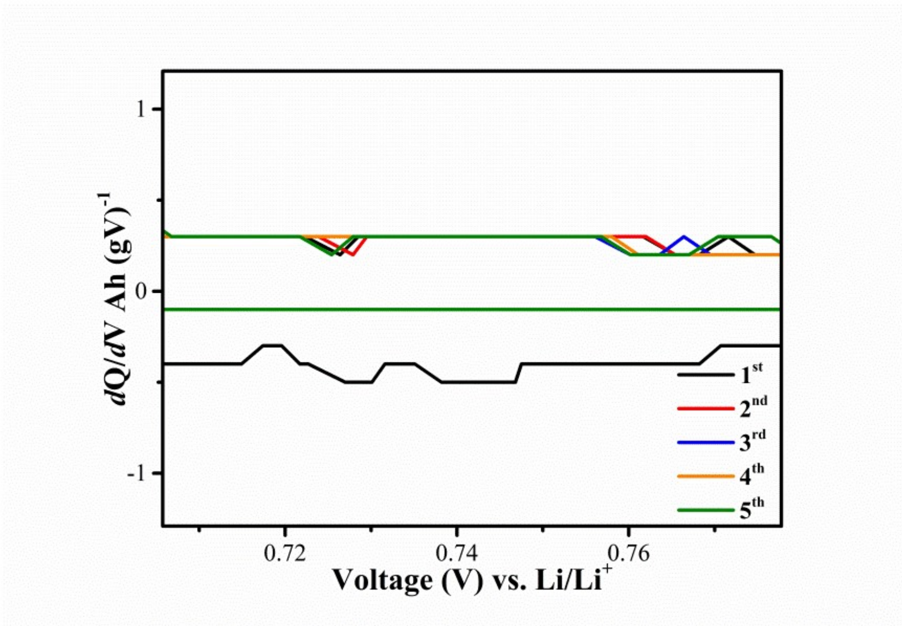

Fig. S17 *Magnified fragment of dQ/dV plots of the Si@FeNO@P.*

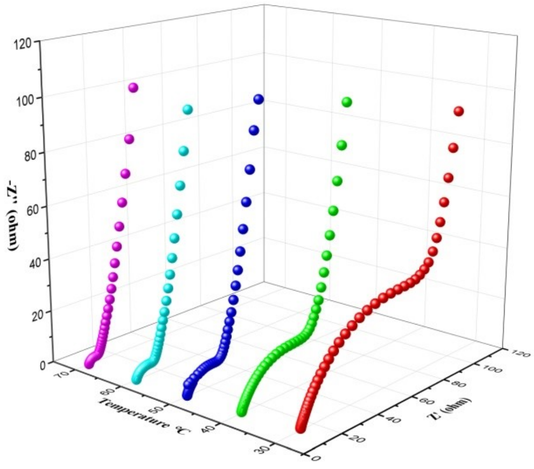

Fig. S18 *EIS plots of the Si electrode at different temperatures.*

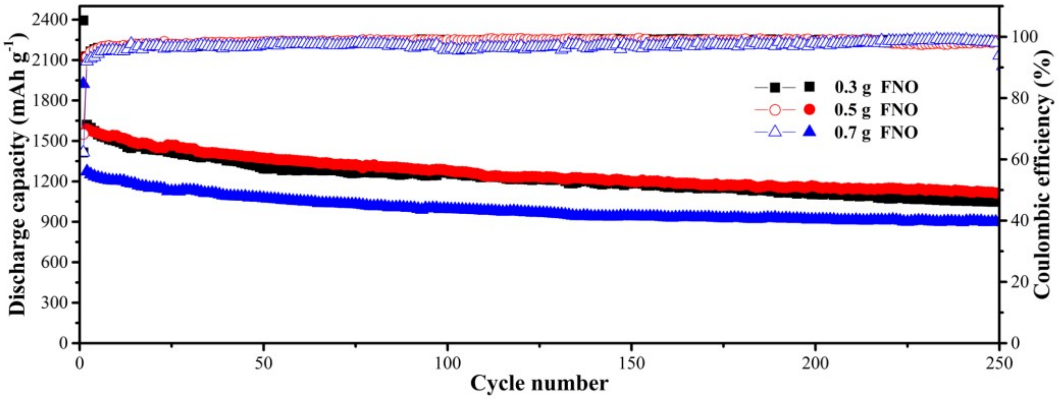

Fig. S19 *Cycling performance of samples prepared with different dosage of $Fe(NO_3)_3$ at 0.1A g^{-1}.*

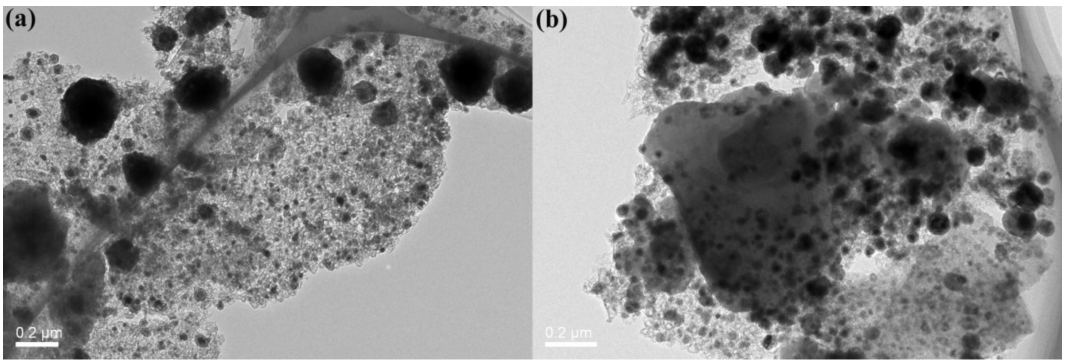

Fig. S20 *TEM images of samples prepared with (a) 0.3 g and (b) 0.7 g of $Fe(NO_3)_3$.*

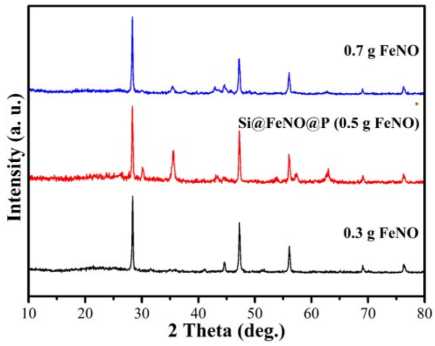

Fig. S21 *XRD patterns of samples prepared with different dosage of $Fe(NO_3)_3$.*

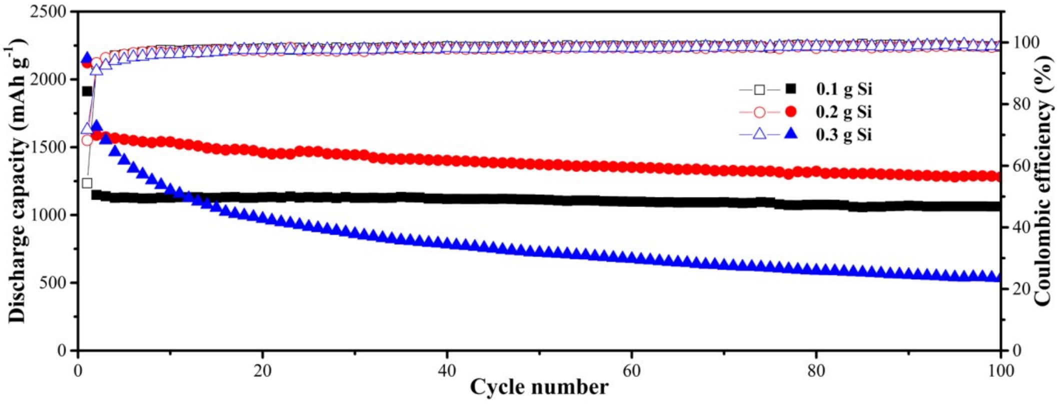

Fig. S22 *Cycling performance of samples prepared with different dosage of Si at 100 mA g^{-1}.*

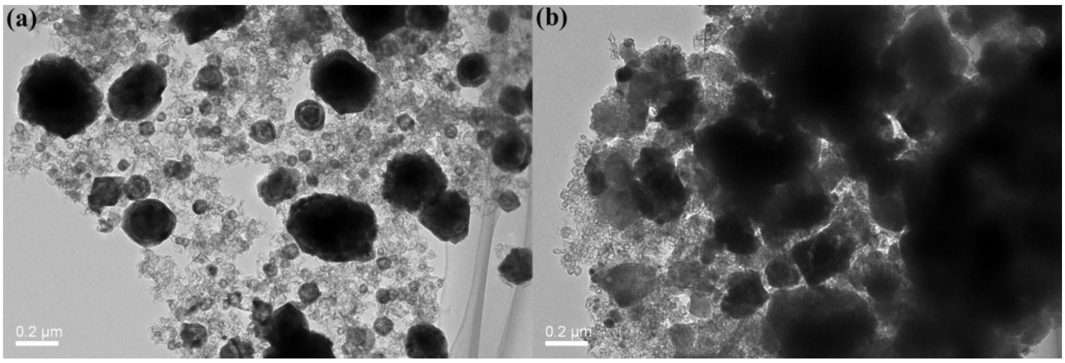

Fig. S23 *TEM images of samples prepared with (a) 0.1 g and (b) 0.3 g of Si.*

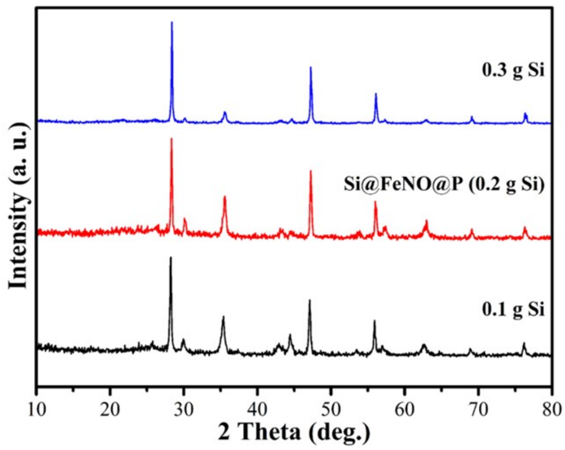

Fig. S24 *XRD patterns of samples prepared with different dosage of Si.*

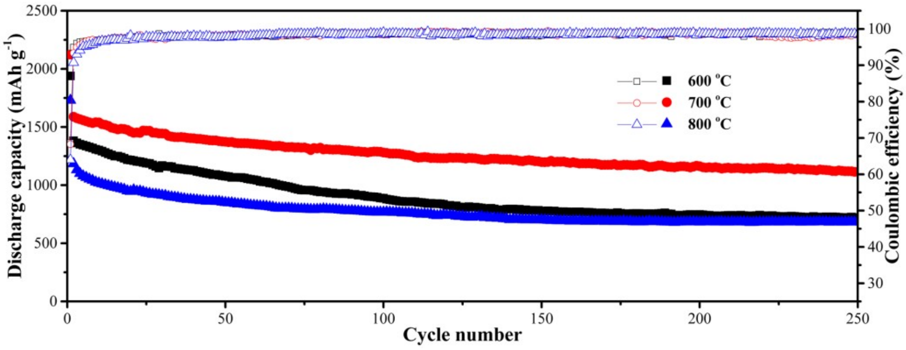

Fig. S25 *Cycling performance of samples prepared with different carbonization temperatures at 100 mA* g^{-1}.

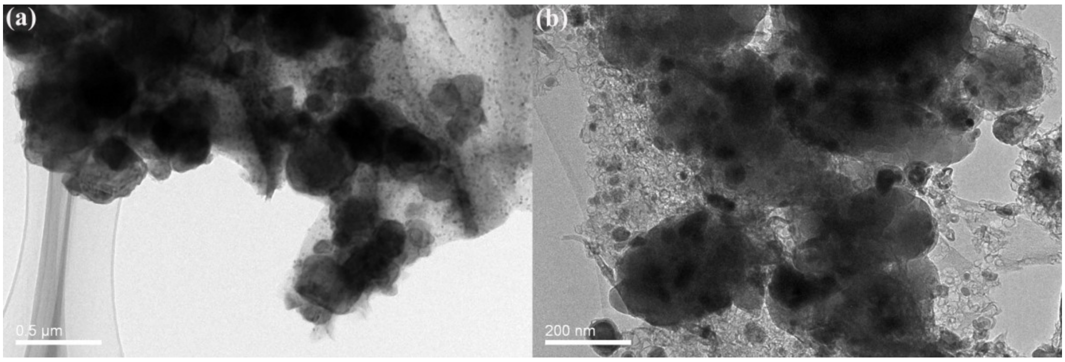

Fig. S26 *TEM images of samples prepared at (a) 600 ℃ and (b) 800 ℃.*

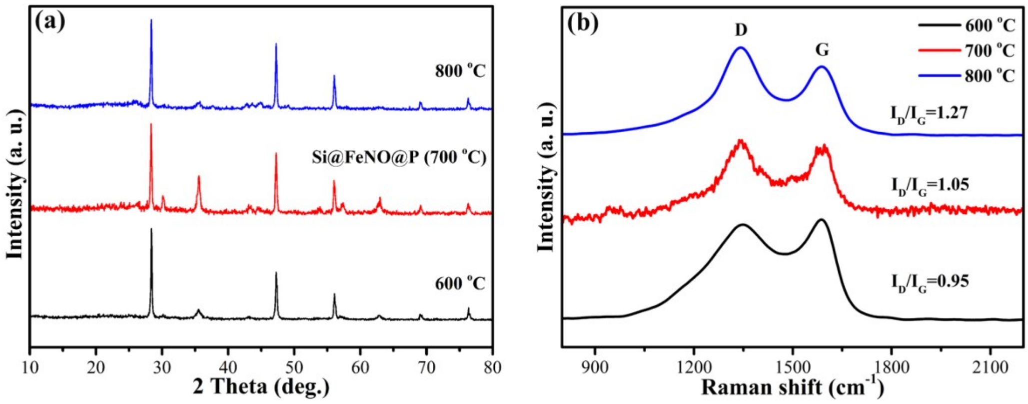

Fig. S27 *(a) XRD patterns and (b) Raman spectra of samples prepared with different carbonization temperatures.*

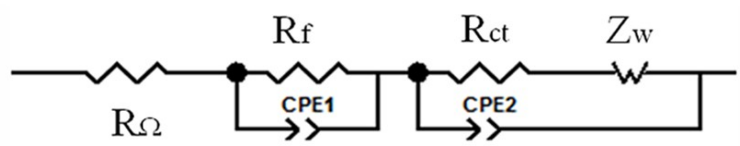

Fig. S28 *An equivalent circuit.*

In the equivalent circuit diagram the R_{Ω}, R_f, R_{ct}, CPE, and Z_w represent the ohmic resistance, ionic resistance at the SEI layer, charge transfer resistance, constant phase-angle element, and Warburg impedance, respectively [26].

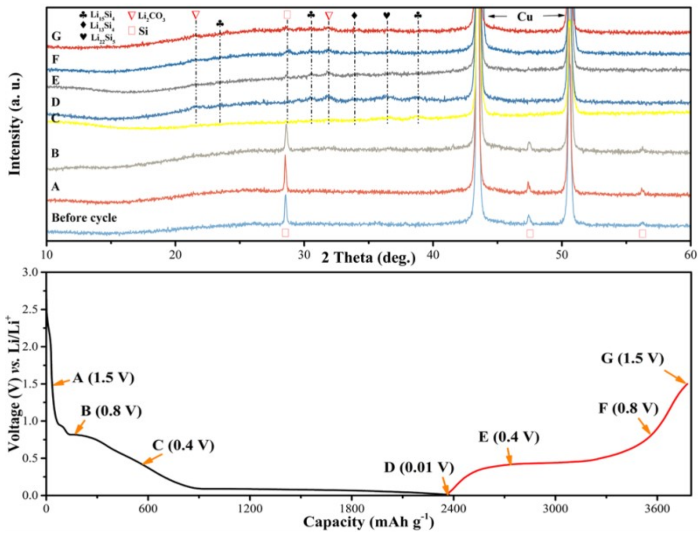

Fig. S29 *XRD patterns of the Si@FeNO@P electrode under different electrochemical states during the first cycle at 100 mA g*$^{-1}$.

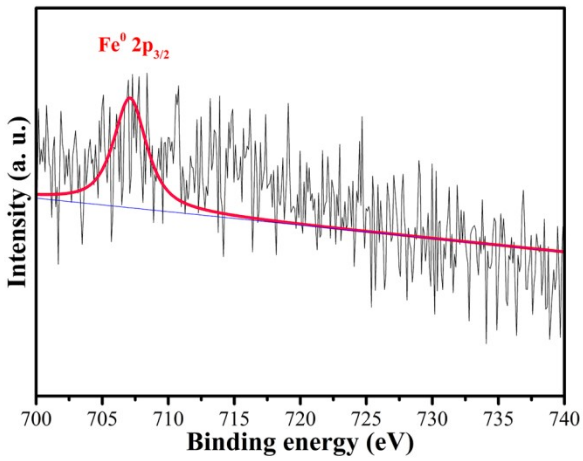

Fig. S30 *High-resolution XPS spectrum of the Fe 2p of the Si@FeNO@P after 50 cycles at 100 mA* g^{-1}.

For assembling full battery, the commercial LFP electrode was employed as the cathode and the as-prepared Si@FeNO@P electrode as the anode. The Si@FeNO@P anodes were activated for two cycles with lithium metal counter electrode at 100 mA g^{-1} between 0.01 and 1.5 V before assembling the full battery. The galvanostatic charge/discharge test of the as-assembled full battery was achieved at 0.1 C between 1 and 4.2 V based on a LAND CT2001a cell test system.

Table S1. *The lithium storage comparison of the Si@FeNO@P with other Si/C-based composites*

Si/C-based anode materials	Potential cutoff (V)	Current density (mAg^{-1})	Cycles	Capacity ($mAhg^{-1}$)	Reference
Si@FeNO@P	1.5-0.01	100	250	1116.1	This work
Si@FeNO@P	1.5-0.01	1000	500	858.1	This work
Si@FeNO@P	1.5-0.01	5000	500	503.1	This work
CNT/Fe@Si@SiO_2	1.0-0.01	1000	500	968	[1]
C/ Si@SnO_2	3.0-0.01	100	200	919.21	[2]
N-doped TiO_2/Si/C	3.0-0.001	100	80	538	[3]
Si@Co–NC	2.0-0.005	100	80	775.5	[4]
Si@Co-C	3.0-0.01	1000	500	650	[5]
Si@C/TiO_2@C/HC	3.0-0.01	1000	400	558	[6]
Si@Fe_2O_3/C	2.0-0.01	1000	300	680.7	[7]
Si@Ni-NP/CNTs	1.5-0.01	100	100	1008	[8]
Si@TiO_2@rGO	3.0-0.01	200	100	1135.1	[9]
Si@TiO_2-B/CNTs	2.5-0.01	200	100	1184	[10]
Si@void C@TiO_2	2.5-0.01	100	500	668	[11]
Si@WO_3@C	3.0-0.01	1000	100	610	[12]
Si/Ge/G@C	3-0.01	100	100	706	[13]
Si-Mn/C	2-0.01	1000	100	960	[14]
Si/Mxene@Zn-C	3-0.01	100	150	862.9	[15]
SiO_x–TiO_2/Si/CNTs	2.5-0.005	100	100	800	[16]
Si/Sb/Sb_2O_3/G@C	3-0.01	1000	180	567.8	[17]
Si/Sn@SiO_x-C	1.5-0.01	500	100	1102	[18]
Si/$TiSi_2$/G@C	1.5-0.01	800	120	943.8	[19]
ZnO/Si/PC	3-0.01	1000	300	500	[20]
T_{12}-Si/C	3-0.01	200	100	1449.2	[21]
Si@LT-4-5	3-0.01	500	150	888	[22]
Graphene/IOC@Si	1.5-0.005	1000	450	484	[23]
Si-M1	1.2-0.1	1000	100	2522.6	[24]
Si@CEG/C	1.5-0.01	1000	200	963.8	[25]

References

[1] M. Zhang, L. Li, X. Jian, et al. Free-standing and flexible CNT/(Fe@Si@SiO_2) composite anodes with kernel-pulp-skin nanostructure for high-performance lithium-ion batteries [J]. J. Alloys Compd., 2021, 878: 160396.

[2] S. Liu, W. Tao, Y. Yu, et al. Ball milling synthesis of robust sandwich-structured C/Si@SnO_2 anode with porous silicon buffer layer for fast charging lithium-ion battery [J].

Colloids Surf., A, 2022, 654: 130088.

[3] S. Xie, Q. Ji, Y. Xia, et al. Mutual performance enhancement within dual n‐doped TiO_2/Si/C nanohybrid lithium‐ion battery anode [J]. ChemistrySelect, 2021, 6(2): 141-53.

[4] Q. Li, Y. Wang, J. Yu, et al. High-performance Si-containing anode materials in lithium-ion batteries: a superstructure of Si@Co–NC composite works effectively [J]. Green Energy Environ., 2022, 7(1): 116-29.

[5] J. Yan, C. Gao, S. Qi, et al. Encapsulation of nano-Si into MOF glass to enhance lithium-ion battery anode performances [J]. Nano Energy, 2022, 103: 107779.

[6] Y. Li, G. Chen, J. Lin, et al. Si@C/TiO_2@C/hollow-C nanocomposite as a lithium-Ion battery anode produced by refining silicon and Ti–6Al–4V residuals [J]. ACS Appl. Energy Mater., 2021, 4(12): 14526-36.

[7] Q. Wang, C. Guo, J. He, et al. Fe_2O_3/C-modified Si nanoparticles as anode material for high-performance lithium-ion batteries [J]. J. Alloys Compd., 2019, 795: 284-90.

[8] Y.-Q. Wang, X.-X. Yang, M.-X. Ren, et al. 3D CNTs networks enable core-shell structured Si@Ni nanoparticle anodes with enhanced reversible capacity and cyclic performance for lithium ion batteries [J]. Int. J. Hydrogen Energy, 2021, 46(29): 16179-87.

[9] R. Fang, C. Miao, H. Mou, et al. Facile synthesis of Si@TiO_2@rGO composite with sandwich-like nanostructure as superior performance anodes for lithium ion batteries [J]. J. Alloys Compd., 2020, 818: 152884.

[10] N. Zhou, Y. Wu, Y. Li, et al. Interconnected structure Si@TiO_2-B/CNTs composite anode applied for high-energy lithium-ion batteries [J]. Appl. Surf. Sci., 2020, 500: 144026.

[11] L. Hou, R. Cui, S. Xiong, et al. A multilayered sturdy shell protects silicon nanoparticle

Si@void C@TiO_2 as an advanced lithium ion battery anode [J]. Phys. Chem. Chem. Phys., 2021, 23(6): 3934-41.

[12] Y. Liu, R. Guo, H. Zhu, et al. A novel propeller-like Si@WO_3@C with boosted electrochemical properties as anode material for lithium-ion batteries [J]. Vacuum, 2021, 184: 109922.

[13] Z. Li, K. Zhang, M. Ma, et al. Facile fabrication of Si/Ge/G@C composite electrodes for high performance lithium-ion batteries [J]. Silicon, 2022.

[14] S. Wang, T. Wang, Y. Zhong, et al. Structure and electrochemical properties of Si-Mn/C core–shell composites for lithium-ion batteries [J]. Jom, 2020, 72(8): 3037-45.

[15] Zhang P, Chen J, Feng L, et al. Dual confinement of Si nanoparticles in a Mxene/ZIF-8-derived carbon framework for lithium-ion batteries[J]. ACS Appl. Nano Mater., 2022, 5(9): 12720-12728.

[16] J. Jiang, Y. Ou, Y. Jiang, et al. Preparation of SiO_x–TiO_2/Si/CNTs composite microspheres as novel anodes for lithium-ion battery with good cycle stability [J]. J. Mater. Sci.: Mater. Electron., 2022, 33(14): 11025-37.

[17] F. Sun, H. Feng, S. Gao, et al. Facile fabrication of Si/Sb/Sb_2O_3/G@C composite electrodes for high-performance li-ion batteries [J]. New J. Chem., 2020, 44(10): 4122-8.

[18] R. Miao, J. Zhu, S. Kang, et al. In-situ mechanochemical synthesis of sub-micro Si/Sn@SiO_x-C composite as high-rate anode material for lithium-ion batteries [J]. Electrochim. Acta, 2021, 384: 138413.

[19] Y. Zhang, M. Chen, Z. Chen, et al. A novel Si/$TiSi_2$/G@C composite as anode material with excellent lithium storage performances [J]. Mater. Lett., 2021, 299: 130078.

[20] X. Sun, J. Gao, C. Wang, et al. A hybrid ZnO/Si/porous-carbon anode for high performance lithium ion battery [J]. Chem. Eng. J., 2020, 383: 123198.

[21] X. Lin, A. Li, D. Li, et al. Facile fabrication of high-performance Si/C anode materials via $AlCl_3$-assisted magnesiothermic reduction of phenyl-rich polyhedral silsesquioxanes [J]. ACS Appl. Mater. Interfaces, 2020, 12: 15202−15210.

[22] M. Liu, H. Gao, G. Hu, et al. Facile preparation of core-shell Si@Li 4 Ti 5 O 12 nanocomposite as large-capacity lithium-ion battery anode [J]. J. Energy Chem., 2020, 40: 89–98.

[23] Y. Lu, Z. Ye, Y. Zhao, et al. Graphene supported double-layer carbon encapsulated silicon for high-performance lithium-ion battery anode materials [J]. Carbon, 2023, 201: 962–971.

[24] J. Tang, F. Wu, X. Dai, Robust MXene adding enables the stable interface of silicon anodes for high-performance Li-ion batteries [J]. Chem. Eng. J., 2023, 452: 139139.

[25] X. Liu, H. T. Liu, Y. H. Cao, et al. Silicon nanoparticles embedded in chemical-expanded graphite through electrostatic attraction for high-performance lithium-Ion batteries, ACS Appl. Mater. Interfaces, https://doi.org/10.1021/acsami.2c21866

[26] X. L. Li, J. F. Zhu, Y. Fang, et al. Hydrothermal preparation of CoO/T_{i3C2} composite material for lithium-ion batteries with enhanced electrochemical performance [J]. J. Electroanal. Chem., 2018, 817: 1-8.

***Table S2** Comparison of lithium storage performance of the as-prepared samples at 100 mA g^{-1}*

Samples	**C content (%)**	**Si content (%)**	**Initial discharge capacity (mAh g^{-1})**	**ICE (%)**	**Reversible capacity (mAh g^{-1})**	**Cycle retention (%)**	**Rate performance (mAh g^{-1}@A g^{-1} at 10th cycle)**
Si	0	～100	3837.7	80.8	460.9 (120 cycles)	12.0	1546.7@0.1 1044.4@0.3 843.3@0.5 633.5@1 442.5@2 335.6@3 834@0.1
Si@P	～48.8	～51.2	1855.9	61.9	680.3 (180 cycles)	36.7	1024.4@0.1 856.9@0.3 753.7@0.5 655.3@1 557.1@2 504.8@3 795.1@0.1
Si@FeNO	0	～67.0	2031.8	61.3	974.5 (159 cycles)	48.0	1287.7@0.1 1127.4@0.3 1021.8@0.5 868.7@1 703.9@2 587.9@3 1106.4@0.1
Si@FeNO@P	～26.2	～44.6	2123.2	68.3	1116.1 (250 cycles)	52.6	1428.2@0.1 1305.6@0.3 1260.5@0.5 1149.8@1 1055.7@2 973.5@3 1260.8@0.1
Si@FeNO@P-Et	～37.2	～62.8	2206.1	69.5	839.5 (175 cycles)	38.1	1401.1@0.1 1226.2@0.3 1121.7@0.5 1011.6@1 881.3@2 771.6@3 1090.3@0.1
FeNO@P	～48.8	0	769.1	28.5	180.3 (250 cycles)	3.7	217.9@0.1 183.6@0.3 167.1@0.5 144.2@1 121@2 104.1@3 206.2@0.1